ACS APPLIED MATERIALS & INTERFACES

Research Article

www.acsami.org

Rolling Silver Nanowire Electrodes: Simultaneously Addressing Adhesion, Roughness, and Conductivity

Tate C. Hauger,[†,‡] S. M. Ibrahim Al-Rafia,[†,‡] and Jillian M. Buriak*[,†,‡]

[†]National Institute for Nanotechnology (NINT), National Research Council, 11421 Saskatchewan Drive, Edmonton, Alberta T6G 2M9, Canada

[‡]Department of Chemistry, University of Alberta, Edmonton, Alberta T6G 2G2, Canada

Supporting Information

ABSTRACT: Silver nanowire mesh electrodes represent a possible mass-manufacturable route toward transparent and flexible electrodes for plastic-based electronics such as organic photovoltaics (OPVs), organic light emitting diodes (OLEDs), and others. Here we describe a route that is based upon spray-coated silver nanowire meshes on polyethylene terephthalate (PET) sheets that are treated with a straightforward combination of heat and pressure to generate electrodes that have low sheet resistance, good optical transmission, that are topologically flat, and adhere well to the PET substrate. The silver nanowire meshes were prepared by spray-coating a solution of silver nanowires onto PET, in air at slightly elevated temperatures. The as-prepared silver nanowire electrodes are highly resistive due to the poor contact between the individual silver nanowires. Light pressure applied with a stainless steel rod, rolled over the as-sprayed silver nanowire meshes on PET with a speed of 10 cm s^{-1} and a pressure of 50 psi, results in silver nanowire mesh arrays with sheet resistances of less than 20 Ω/□. Bending of these rolled nanowire meshes on PET with different radii of curvature, from 50 to 0.625 mm, showed no degradation of the conductivity of the electrodes, as shown by the constant sheet resistance before and after bending. Repeated bending (100 times) around a rod with a radius of curvature of 1 mm also showed no increase in the sheet resistance, demonstrating good adherence and no signs of delamination of the nanowire mesh array. The diffuse and direct transmittance of the silver nanowires (both rolled and as-sprayed) was measured for wavelengths from 350 to 1200 nm, and the diffuse transmission was similar to that of the PET substrate; the direct transmission decreases by about 7−8%. The silver nanowires were then incorporated into OPV devices with the following architecture: transparent electrode/PEDOT:PSS/P3HT:PC_{61}BM/LiF/Al. While slightly lower in efficiency than the standard indium tin oxide substrate (ITO), the rolled silver nanowire electrodes had a very good device yield, showing that short circuits resulting from the silver nanowire electrodes can be successfully avoided by this rolling approach.

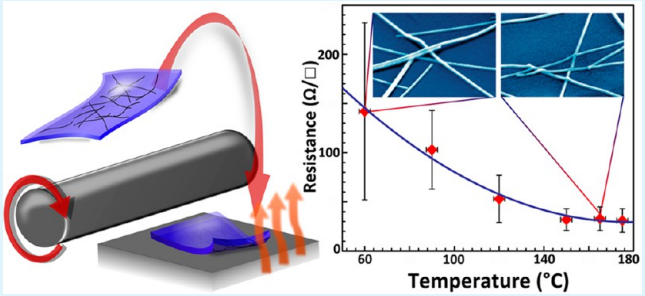

KEYWORDS: *silver nanowire, spray coating, adhesion, conductivity, topology, rolling, transparency, flexible electronics*

1. INTRODUCTION

With the rapid growth of research in flexible electronics, there is enormous demand for both transparent and reflective bendable electrodes.[1−3] Applications include lightweight polymer and small molecule based organic photovoltaics (OPVs), organic light emitting diodes (OLEDs), and displays.[4] The inorganic semiconductor, indium tin oxide (ITO), is the most widely used material as the transparent conducting electrode, but the lack of flexibility and rising price due to limited earth abundance underscore the need for a bendable replacement with low processing cost.[5−8] A number of possible solutions have been proposed, based on metallic and carbon-based nanomaterials that have higher ductility than a typical metal oxide.[1,9−13] Metals are obviously much more flexible than ceramic ITO electrodes, particularly at the nanoscale, and thus, a variety of morphologies and architectures have been investigated. To render a metal at least partially optically transparent, it must be a very thin in at least one dimension. Building on the concept of nanoscale metals, there has been prior work focusing on metal films with thicknesses less than 10 nm,[14,15] and metal grids and nanowire meshes that block or reflect only a small fraction of the incoming or outgoing light[16] Metallic nanowire meshes are simple to produce and very scalable, since the nanowires can be mass-produced using solution-based methods,[17,18] and integrated with a flexible plastic substrate.[19,20] Silver nanowires are most commonly used, but new copper- and nickel-based materials are also showing promise.[21] With respect to the more widely studied silver nanowire workhorse material, this system has been tested as a transparent electrode using production methods as diverse as Meyer rod spreading,[17] spin-, drop-, and dip-coating,[19,22,23] lamination,[23−25] spray-coating,[26] and doctor-blading,[27] among

Received: September 16, 2013
Accepted: November 7, 2013
Published: November 13, 2013

others. Silver nanowires have also been integrated with polymers, such as polyvinyl alcohol,[28] polydopamine,[29] poly(acrylic acid),[30] and PEDOT:PSS,[16,31,32] and with other semiconductor oxides.[7,33−35] Silver and other metallic nanowires are also of interest for their potential to enhance device efficiencies due to plasmonic effects.[36] When all these features are considered together, silver nanowire meshes present many advantages to justify further study.

While silver nanowire meshes are promising due to the potential for the scale-up necessary for mass-manufacturing, there remain a number of significant challenges associated with their use, most notably topological roughness that leads to short-circuits (shunts) between the two electrodes,[19] and poor adhesion to the underlying electrode.[1,17] Sufficient optical transmissivities (>80%) and conductivities (better than 20 Ω/□) have now been repeatedly demonstrated for silver nanowire-based electrodes,[17,19−27] but scale-up to large-scale manufacturing has been stymied by lack of progress with respect to the "pressing processing issues"[1] of roughness and adhesion. In this paper, we demonstrate how rolling with pressure and heat *simultaneously* addresses the important trifecta of nanowire welding, adhesion to the underlying substrate, and lowering surface of roughness via a process that is enabled through a roll-to-roll (R2R) processing step, while attaining expected conductivity and optical transmissivity. A nanowire mesh on a PET substrate, when rolled at a temperature that is above the VICAT softening temperature, brings about nanowire welding, presses the nanowires into the substrate to bring about enhanced physical adhesion, and lowers the surface roughness, in a process that is complete in seconds.

2. EXPERIMENTAL METHODS

Materials. Polyethylene terephthalate (PET) film substrates of 100 μm thickness were provided by SABIC; the T_g of the PET film was reported to be 75 °C. Lithium fluoride (LiF), silver chloride (AgCl), potassium bromide (KBr), silver nitrate ($AgNO_3$), polyvinylpyrrolidone (PVP), and ethylene glycol were purchased from Sigma Aldrich and used without further purification. Solvents were purchased from available commercial sources and used as received unless mentioned otherwise. Aluminum came in pellets from Kurt J. Lesker. For the active layer of the OPV devices, the $PC_{61}BM$ and P3HT were purchased from American Dye Source and Reike Metals Inc., respectively. PEDOT:PSS (PVP AI 4083) was purchased from Heraeus. ITO was puchased from Delta Technologies and had a sheet resistance of 8 − 12 Ω/□. Before OPV fabrication, the ITO was cleaned via 10 min successive sonication treatments in methylene chloride, deionized water, and IPA, followed by a 10 min exposure to an air plasma with a base pressure of 0.8−1.2 Torr.

Synthesis of Silver Nanowires. Silver nanowires were synthesized following literature procedures with slight modifications to the reaction time and purification procedures.[17−19] A typical synthesis involves reaction of a mixture of 1.32 g of polyvinylpyrrolidone (PVP, average molecular weight 55 000) and KBr (0.040 g, 0.034 mmol) in 75 mL of ethylene glycol heated at 173 °C in a pear shaped three-necked flask for 90 min with constant magnetic stirring (~1200 rpm). After attaining a stable solution temperature, finely ground AgCl (0.21 g, 1.40 mmol) was added to the mixture to initiate nucleation of the silver seeds. After about 5 min, a solution of $AgNO_3$ (0.88 g, 5.18 mmol in 8 mL of ethylene glycol) was added to the reaction mixture over 15 min. Afterward, the resulting mixture was heated at 173 °C for an additional 4 h and then allowed to settle at room temperature for 72 h. During this period, the silver nanowires precipitated at the bottom of the flask while other various shapes of nanostructures such as cubes, rods, and spheres remained in the supernatant and were decanted from the reaction flask. The remaining silver nanowire precipitate was then dispersed into 70 mL of methanol and centrifuged twice at 2500 rpm for 40 min to remove ethylene glycol, PVP, and other impurities. Finally, uniform silver nanowires were dispersed in 30 mL of methanol.

Silver Nanowire Mesh Preparation. Before processing, the PET substrates were cleaned by rinsing in a 1:1 acetone/IPA mixture for approximately 5 s, wiping with a Kimtec kimwipe tissue, rinsing again with the acetone/IPA, and then blown dry with nitrogen. All spray-coating was carried out using a Sono-Tek ExactaCoat SC ultrasonic spray-coating system in an ambient atmospheric environment. For all samples, the ultrasonic tip vibrated at 60 kHz with a power of 1.0 W at a height 55 mm above the sample, which rested on a heated plate. The temperature of the heated plate was set to the desired temperature before spraying and allowed to stabilize. A 5 mg/mL solution concentration was used for all samples with a solution flow rate of 800 μL/min. Argon at a set pressure of 17 kPa was used as flowing gas to control the shape of the deposited film. The nozzle was rastered over the entire length of a substrate horizontally at a speed of 50 mm/s and offset 4 mm perpendicularly to the substrate between each pass. Upon completion of one full raster cycle, the pattern was repeated but shifted perpendicularly 2 mm on each pass to ensure a uniform film. When both raster patterns were completed, the coated PET was removed from the spray-coating system and placed face down on a piece of polished stainless steel (0.8 mm thick), sitting on a hot plate at the desired temperature. A custom-made stainless steel roller with a radius of 30 mm and length of 150 mm was then rolled on the back of the PET. Six passes of the roller (6 × one roll) was carried out to ensure that the entire substrate had been processed with an equal amount of pressure. The substrates prepared for these experiments ranged in size from a length of 75 to 150 mm and a width of 15 ± 2 mm.

Assembly of the P3HT/$PC_{61}BM$ OPV Devices. In a nitrogen-filled glovebox, 25 mg of P3HT and $PC_{61}BM$ were placed in separate vials followed by 500 μL of *o*-dichlorobenzene to each vial. After stirring on a hot plate at 80 °C overnight, the $PC_{61}BM$ solution was added to the P3HT solution and allowed to stir for 2 h in the glovebox before being removed for spin coating in air. The resulting solution was 1:1 w/w of P3HT:$PC_{61}BM$ solution with a concentration of 25 mg/mL of each constituent. On each transparent electrode (ITO or silver nanowire mesh), a PEDOT:PSS layer was spin-cast in air at 4000 rpm for 60 s, followed by the active layer that was spin-coated at 600 rpm for 60 s. The film was allowed to dry in a plastic Petri dish until a change in color from orange to purple color was observed. Upon drying, the film was loaded into the glovebox and pumped down to a base pressure of 5×10^{-6} mbar for thermal evaporation of the LiF (0.8 nm) and Al (80 nm) top electrode.

Characterization. Sheet resistance was measured using a Keithley 2400 source meter in conjunction with a Jandel 4 point probe unit, and values reported are taken to be the average of a minimum of 8−10 measurements from random parts of the substrate unless otherwise stated. UV−vis spectra were taken on a Perkin-Elmer Lambda 900 spectrophotometer operating in normal mode. For diffuse transmission measurements, the same UV−vis spectrometer was used with an integrating sphere and an incident beam at a normal angle to the surface of the substrate. The transmitted light was then captured and measured by an integrating sphere. The transmission data has been corrected for the PET substrate, unless otherwise stated. Atomic force microscopy (AFM) was performed in tapping mode on a Digital Instruments/Veeco multimode tapping atomic force microscope, and the collected data was analyzed using the open source software, Gwyddion. Scanning electron microscopy (SEM) images were taken using a Hitachi S4800 high resolution microscope with a beam current of 20 μA and an accelerating voltage between 1 and 15 kV. Samples on PET had a thin layer (5 nm) of gold sputtered on top to assist with imaging. Pressure was determined by rolling the stainless steel roller over Fujifilm Prescape tactile pressure-indicating film in an identical manner to the rolling of the silver nanowires, at room temperature. Upon the application of pressure, the Fujifilm changes color to quantify the applied pressure. This color change was compared against the color-calibrated indicator, and the pressure was determined. The tactile film was cut to the same dimensions as the PET substrates, as

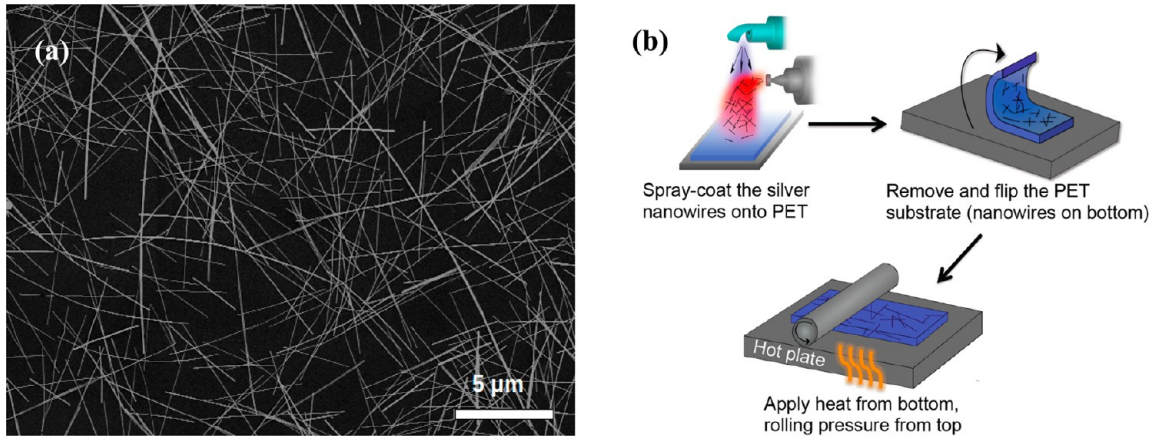

Figure 1. Outline of the process for rolling the silver nanowire mesh electrode. (a) SEM image of the silver nanowires used in this study. (b) Silver nanowires are spray-coated onto a PET substrate. After drying, the PET substrate is inverted on a hot plate (silver nanowires are in contact with the hot plate surface) at the desired temperature, followed by rolling with a steel rod.

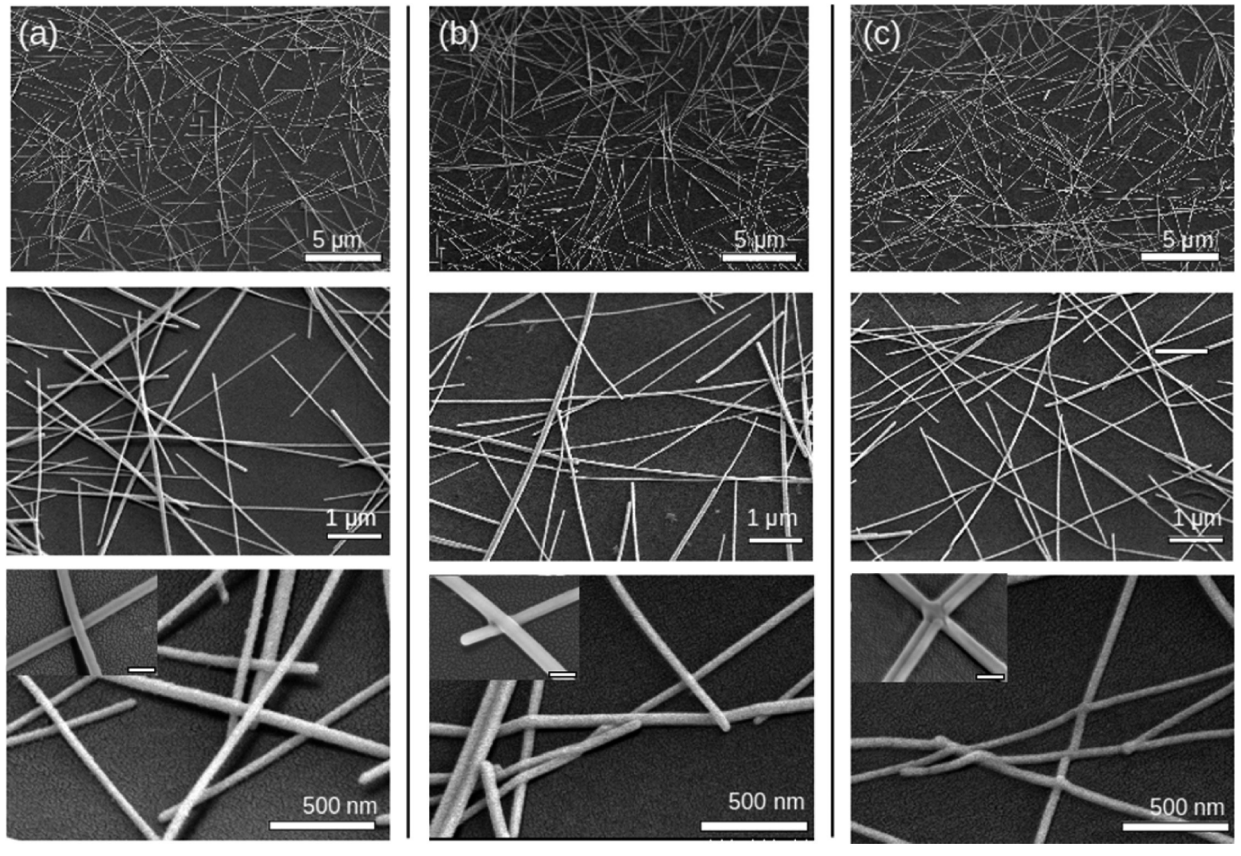

Figure 2. SEM images of silver nanowires spray coated onto SABIC PET; each sample was imaged at three different magnifications. (a) Silver nanowires spray-coated at 60 °C without rolling. (b) Silver nanowires both spray-coated and rolled at 60 °C. (c) Silver nanowires spray-coated at 60 °C and rolled at 165 °C. The insets in the bottom series show higher resolution images of nanowire junctions; the scale bar for the inset images is 100 nm.

pressure is size dependent. Keeping the substrate width constant and using only the weight of the roller allowed for reproducible pressure applicability. Higher pressures were estimated by pushing on the roller with a force that is approximately 4 times that exerted by the weight of the roller alone, and confirming with the Fujifilm indicating-film. OPV performance was evaluated using custom designed software to interface with a Keithley 2400 source meter and a OAI Trisol 300 W AAA solar simulator. The light intensity was set against a Si reference cell from PV Measurements Inc., model number PVM624, fitted with a KG5 filter. This calibration was carried out at the beginning of each test.

3. RESULTS AND DISCUSSION

In this work, silver nanowire meshes were prepared on PET substrates via spray-coating, followed by a thermal rolling process. While the focus of this work is on silver nanowires, the thermal rolling should be applicable to any metal nanowire mesh, regardless of its method of production (i.e., spin-coating,

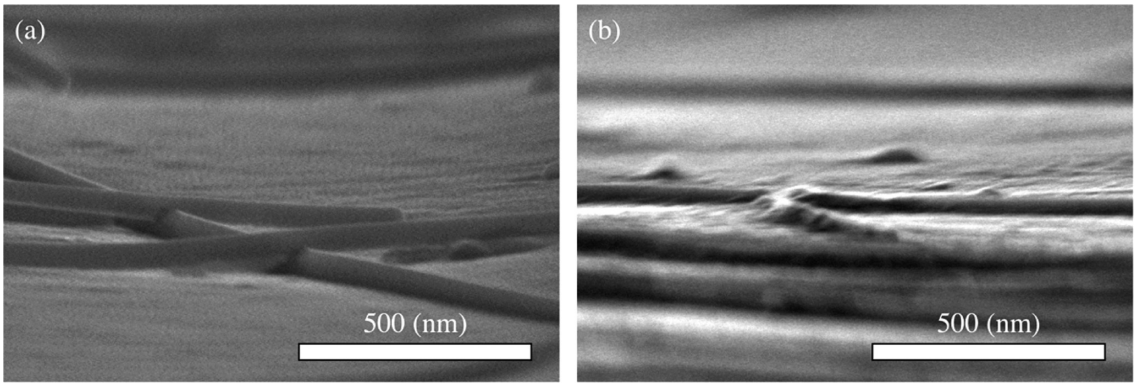

Figure 3. SEM images taken at an angle of 85° to illuminate the morphological differences between silver nanowire mesh samples: (a) as-sprayed and (b) a sample rolled at 165 °C.

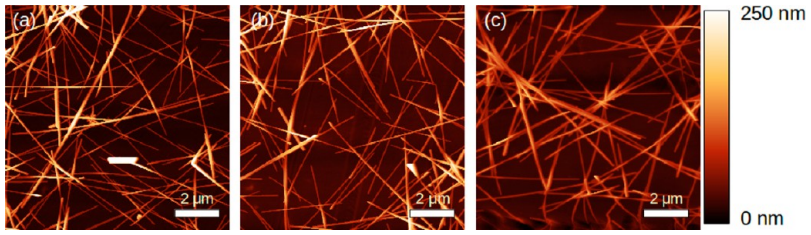

Figure 4. AFM images of silver nanowire mesh on PET. The silver nanowires were all sprayed at 800 μL/min with a head speed of 50 mm/s and a step size of 4 mm. The solution concentration was 5 mg/mL in methanol. The AFM images were taken with a very slow scan speed of 0.25 Hz, and the images are displayed with a height scale bar (*z*-scale) of 0−250 nm for all images; all images are 10 μm by 10 μm. (a) Nanowires as sprayed at 60 °C. (b) Nanowires sprayed and rolled at 60 °C. (c) Nanowires sprayed at 60 °C and rolled at 165 °C.

doctor-blading, and other processes). The application of pressure to flatten silver nanowire meshes has received some investigation. For instance, Peumans and co-workers drop-cast a silver nanowire suspension onto glass, which leads to a very rough and almost hairy-looking silver nanowire material; when pressed onto a smooth film of PEDOT:PSS with a pressure of 2.4×10^4 psi, the nanowires were transferred onto the PEDOT:PSS, and had a much flatter profile.[23] Pressures of up to 81 GPa (1.1×10^7 pounds per square inch, psi) have also been shown to flatten silver nanowire meshes and improve conductivity.[17] Coleman and co-workers used vacuum filtration of a silver nanowire suspension to prepare a film, which was then transferred onto PET by placing the silver nanowires in contact with PET under weight for 2 h.[20] In this work, rapid (seconds) application of a roller at a pressure of 50 psi at 165 °C were shown to enable the production of flattened silver nanowire meshes with high conductivity and excellent adhesion on PET substrates. Silver nanowires with diameters of 50−100 nm and lengths of 5−10 μm were prepared via a straightforward solution phase procedure.[17] A representative example of a spray-coated silver nanowire mesh on PET is shown in the SEM image in Figure 1a. The commercial PET films from SABIC were 100 μm thick, with a reported T_g of 75 °C and a VICAT softening temperature of 79 °C. Figure 1b provides the schematic outline of the electrode processing described: The silver nanowires were spray-coated onto cleaned PET, removed from the spray-coater, and turned over onto a polished stainless steel hot plate with the nanowires in contact with the hot plate surface at the desired temperature. The back of the PET film was then rolled with a stainless steel rod (radius = 30 mm) a specified number of times (1−6 times) and then removed and allowed to rapidly cool. If not stated, the stainless steel rod was passed over the substrate six times at a speed of 10 cm s^{-1} at a measured pressure of 50 psi. The electrodes were then analyzed through a variety of techniques, including SEM and AFM, transmission and conductivity measurements, bending tests, and finally incorporation into OPV devices.

Examples of silver nanowire meshes on PET substrates are shown in the low-, medium-, and higher-resolution SEM images in Figure 2. A silver nanowire mesh that was sprayed but had no further treatment can be seen in Figure 2a, and it appears that the rigid rods or wires overlap, with some not in obvious physical contact with the underlying PET. In Figure 2b, rolling the wires on the surface heated to 60 °C results in some flattening of the wires with respect to the substrate surface, but no obvious welding at nanowire junctions. At a higher temperature, 165 °C, as shown in Figure 2c, the nanowires have welded together at their intersection points. Close-up images of junctions are shown in the inset SEM images of Figure 2 to demonstrate the welding. It is assumed that when the wires make contact with the hot plate at 165 °C, thermal energy is transferred through the nanowires to the plastic substrate where they heat the plastic locally to temperatures above the VICAT softening point. The heat combined with the pressure from the roller allows the wires to be slightly pressed into the substrate and become attached. SEM images of highly tilted samples (85°) in Figure 3 show an untreated, spray-coated silver nanowire mesh on PET (Figure 3a), and a silver nanowire mesh that was rolled at 165 °C and 50 psi (Figure 3b). As can be seen, the rolled silver nanowires in Figure 3b are less distinct because they have been pressed into the underlying PET, and are challenging to image by SEM as compared to the unrolled sample in Figure 3a.

To further study the effect of rolling temperature on morphology, AFM images where taken and analyzed for the three samples shown in Figure 2 (Figure 4). The measured rms

roughness values are provided (Table 1), and the corrected rms roughness that takes into account the percent surface coverage

Table 1. Summary of the Roughness Calculations, Based upon the AFM data from Figure 4[a]

sample	roughness (nm rms)	surface coverage (%)	normalized roughness (nm rms)
unrolled	43	40%	107
60 °C	36	37%	97
165 °C	27	38%	71

[a]The as-determined roughness is also reported with the normalized roughness, which has been corrected for surface coverage.

(40, 37, and 38%, respectively). As can be seen, the normalized rms roughness drops to 71 nm upon rolling at 165 °C and 50 psi. More detailed information on the normalized roughness values and area coverage can be found in the Supporting Information.

To better understand the effects of the different parameters of the processing applied to these silver nanowire meshes, the effects of temperature, pressure, and rolling speed were deconvoluted. Table 2 shows the results for spray-coated silver

Table 2. Resistance of Different Substrates and Processes Sprayed under the Same Conditions (800 μl/min, 60 °C, 2 passes, 5 mg/mL)

substrate	resistance (Ω/□)
glass	2400 ± 1020
glass, rolled at 165 °C	484 ± 202
PET	5800 ± 1200
PET, rolled at 165 °C	17.5 ± 202
PET, annealed at 165 °C	174 ± 133

nanowire mesh electrodes, prepared on both glass and PET substrates; the nanowires were deposited in an identical manner in all cases. The silver nanowires on glass or PET with neither rolling nor annealing are highly resistive, with measured sheet resistances of 2400 and 5800 Ω/□, respectively. Rolling the silver nanowires on glass at 165 °C results in a drop of sheet resistance by about an order of magnitude, but it is on PET that the effects are most obvious. On PET, rolling at 165 °C leads to an observed drop in sheet resistance to 17.5 ± 2.2 Ω/□. The sheet resistance for the nanowire mesh on PET placed face-down on the hot plate at 165 °C for the same length time, without rolling, is 174 ± 33 Ω/□, about an order of magnitude greater than that of the rolled sample, keeping the temperature constant. As summarized in Figure 5 for silver nanowires on PET, the sheet resistances drop with an increase in temperature at which the hot plate is held while the sample is rolled. More importantly from a manufacturability perspective, the standard deviation for the measured sheet resistances drops substantially; above a rolling temperature of 150 °C, the sheet resistance is consistently below 50 Ω/□, whereas at a lower temperature of 60 °C, the sheet resistance varies much more dramatically, from just over 50 to 230 Ω/□. These welding results are in line with prior literature results where temperatures in excess of 150 °C are typically required to anneal the silver nanowire junctions.[37,38]

The influence of speed and pressure on the sheet resistance is subtle (Table 3). When silver nanowire meshes on PET were

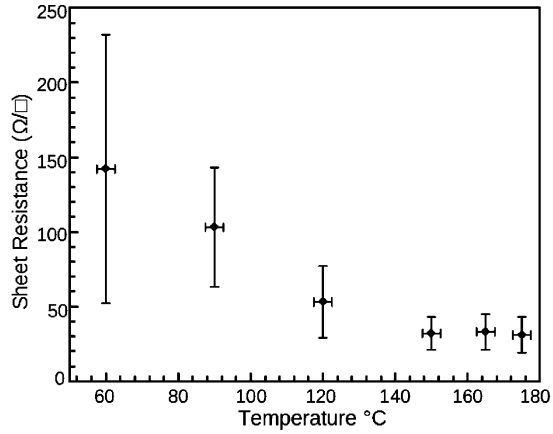

Figure 5. Comparison of the conductivity of the silver nanowire meshes versus against the temperature at which they were rolled. All spraying of the initial silver nanowire meshes on PET was carried out at 60 °C.

Table 3. Effect of Pressure and Rolling Speed on the Sheet Resistance of Silver Nanowire Meshes on PET

substrate	speed (cm/s)	pressure (psi)	resistance (Ω/□)
annealed at 165 °C			370 ± 130
rolled at 165 °C	10 ± 2	50 ± 25	36 ± 3
rolled at 165 °C	1 ± 2	50 ± 25	35 ± 15
rolled at 165 °C	10 ± 2	250 ± 50	173 ± 83
rolled at 165 °C	1 ± 2	250 ± 50	open circuit

examined, it was found that rapid speeds (10 cm/s) at 50 psi resulted in the lowest measured sheet resistance of 26 ± 3 Ω/□ at a temperature of 165 °C. Slower speeds of 1 cm/s at 165 °C led to sheet resistances of 35 ± 3 Ω/□, which is within experimental error, but the measured standard deviation is somewhat greater. Higher pressures produced silver nanowire meshes with substantially higher sheet resistances, including open circuit (nonconductive) films when high pressures (250 psi) and slow speeds are applied at 165 °C. SEM imaging provides an explanation for the damaging effects of high pressure. As can be seen in Figure 6a,b, 50 psi and 1 and 10 cm/s speeds produce continuous nanowire arrays that are in continuous contact with the underlying PET. At higher pressures, on the other hand (Figure 6c,d), the empty impressions or trenches of the same dimensions as the silver nanowires suggest that they have been removed, leaving a discontinuous network of wires through which current cannot flow in an unimpeded fashion. Therefore, the ideal conditions for rolling the nanowire arrays are, within the range of pressures and speeds tested here, lighter pressure and faster rolling. Under these conditions, the pressure is sufficient to press the nanowires onto the PET, but not too hard to damage the wires themselves.

Adherence of the nanowire meshes to the underlying PET was measured in two ways. First, the standard scotch tape test was applied, in which a piece of scotch tape is pressed firmly onto the nanowire mesh on PET by hand and then peeled off. Table 4 shows that, for a sprayed silver nanowire mesh with no rolling or other treatment, the sheet resistance increases from 370 ± 137 Ω/□ to open circuit; the nanowires are presumably removed or disrupted to such an extent that the substrate becomes an insulator. The sample rolled at 165 °C, however, shows an increase in sheet resistance from 37 ± 9 Ω/□ to 167

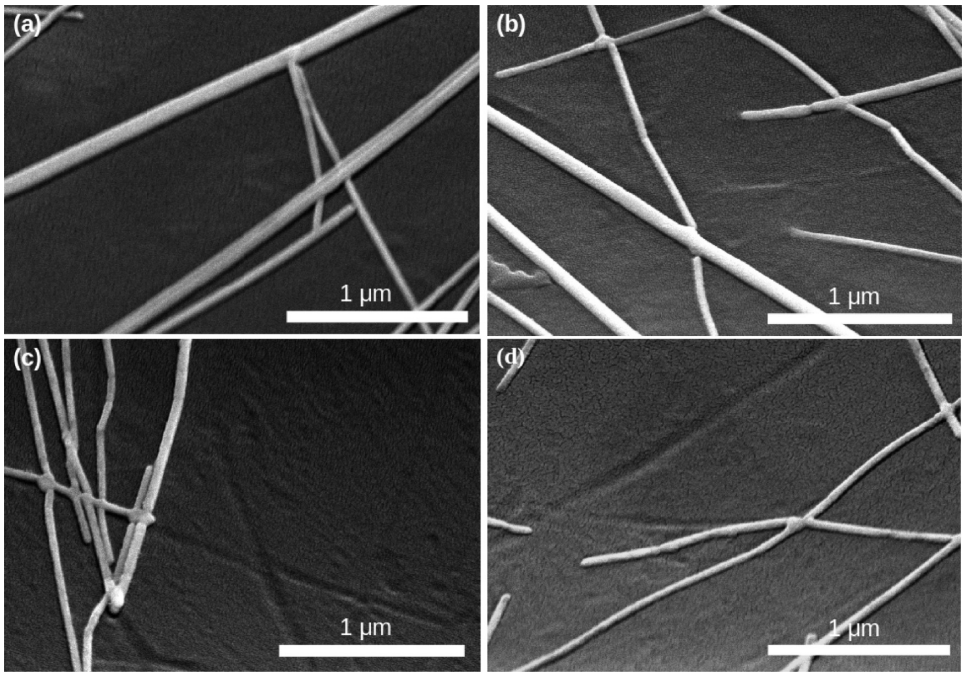

Figure 6. SEM images of silver nanowire meshes on PET substrates. (a,b) Images showing silver nanowires rolled at 50 psi at speeds of (a) 10 cm/s and (b) 1 cm/s. (c, d) Images showing the silver nanowires rolled at a pressure of approximately 250 psi at speeds of (c) 10 cm/s and (d) 1 cm/s.

Table 4. Scotch Tape Testing Applied to Silver Nanowire Mesh Samples As-Deposited and Rolled at 165 °C

substrate treatment	pre-tape (Ω/□)	post-tape (Ω/□)
as-deposited	370 ± 137	open circuit
rolled	37 ± 9	167 ± 40

± 40 Ω/□. The second test of adherence of the silver nanowires to the PET substrate following rolling was demonstrated through a bending test, in which the flexible substrate was bent around rods of various radii of curvature. Figure 7 shows that at all the radii of curvature tested (50–0.625 mm), the sheet resistance of the silver nanowire meshes rolled at 165 °C remains constant below 20 Ω/□. On the other hand, sprayed silver nanowires that were not rolled had a higher overall sheet resistance, which increased substantially when the radius of curvature dropped below 1.0 mm. Clearly, the silver nanowires adhere strongly to the PET substrate after rolling at this temperature, whereas the as-sprayed films are damaged, most likely due to delamination. Even after 100 bending cycles (Figure 7, inset), the silver nanowire meshes rolled at 165 °C maintained their low sheet resistance.

For applications as a transparent or translucent electrode in OPV and OLED devices, conductivity measurements must be supplemented by optical transmissivity studies. Normal and diffuse transmission measurements can provide important information regarding the utility of these nanowire mesh electrodes in architectures that have the requirement of handling light. As can be seen in Figure 8, the direct and

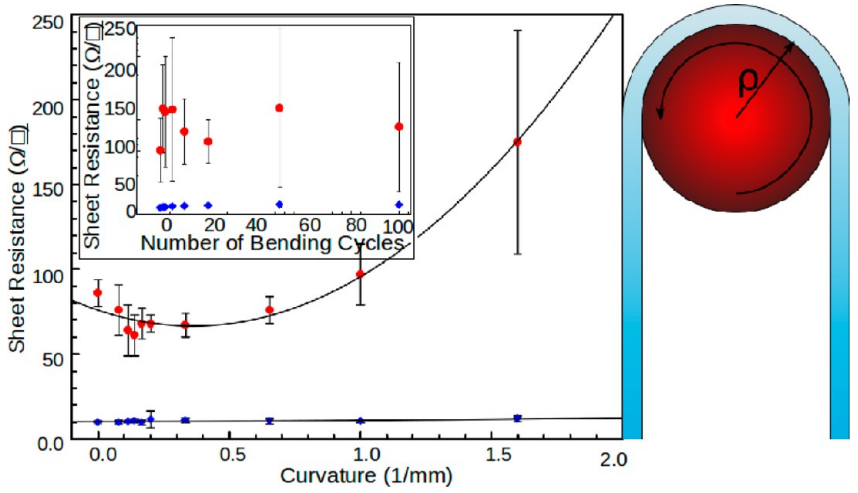

Figure 7. Sheet resistance versus bending of a sample around a given radius of curvature for as-sprayed silver nanowire samples on PET (red) and silver nanowire meshes rolled at 165 °C (blue). The inset shows data for the sheet resistance of each sample after the specified number of bending cycles at a radius of curvature of 1 mm. Each data point is the result of five measurements across each sample.

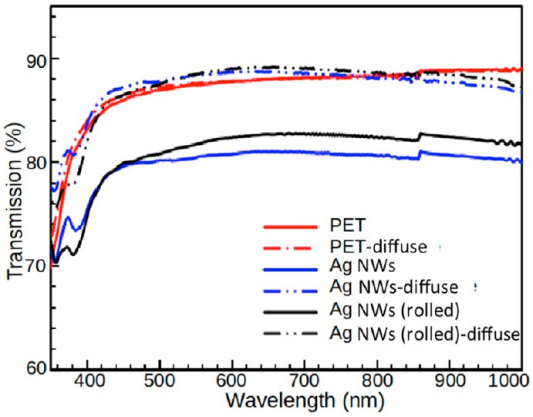

Figure 8. Normal and total transmission profiles of the PET substrate (red), the as-sprayed silver nanowires on PET (blue), and the nanowires on PET that were rolled at 165 °C (black).

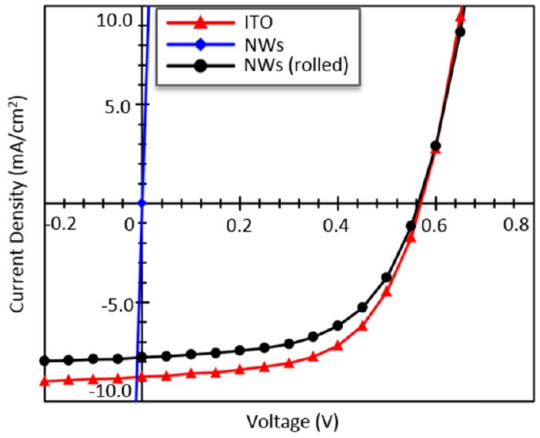

Figure 9. *I*–*V* curves for transparent electrode/PEDOT:PSS/P3HT:$PC_{61}BM$/LiF/Al OPV cells, where the transparent electrode is ITO or silver nanowires on PET (Ag NWs).

diffuse transmissions through the PET substrates (red curves) are almost identical, with the diffuse tranmission increasing slightly over the direct at wavelengths below 550 nm, and ranges from 80% to 87% when weighted equally over the wavelengths of 350–1200 nm. Spectra corresponding to the total transmittance through the PET (uncorrected for a PET background) are shown in the Supporting Information. In the case of the silver nanowire meshes, these samples had measured sheet resistances of 185 ± 96 Ω/□ and 13 ± 2 Ω/□ for the as-sprayed and rolled (at 165 °C) samples, respectively. For both sets of nanowire electrodes (both as-sprayed and rolled), the diffuse transmission is almost identical to that of the parent PET substrate, and the direct transmission is about 7% lower. The figures of merit (FOM) for the rolled silver nanowire electrodes samples are 122 and 201 for normal and diffuse transmission, respectively, calculated using the following equation that compares the ratio of electrical conductivity to optical conductivity where 188.5 Ω is half the impedance of free space, R_s is the sheet resistance, and T is the transmission. A figure-of-merit applicable to industry standards is 220.[39]

$$\mathrm{FOM} = \frac{188.5\ \Omega}{R_s(T^{-1/2} - 1)}$$

In order to demonstrate the applicability of these rolled nanowire mesh electrodes in organic electrodes, a small series of OPV cells were produced based upon the following architecture: PET/Ag nanowires/PEDOT:PSS/P3HT:$PC_{61}BM$/LiF/Al (Figure 9, Table 5). As can be seen, entry 1, the ITO standard cell, demonstrated a PCE of 2.9 ± 0.3% and a J_{sc} of 8.7 ± 0.6 mA/cm^2. The as-sprayed silver nanowire mesh electrodes (no rolling treatment) on PET did not function (entry 2), and had a PCE of 0% initially resulting from an extremely low shunt resistance. This low shunt resistance is indicative of devices failing due to a short between the two electrodes. Entry 3, the rolled silver nanowire mesh electrode, demonstrated a PCE of 2.5 ± 0.3% and a J_{sc} of 8.0 ± 0.6 mA/cm^2. The comparison "standard" cell, based upon ITO, entry 1, had a superior power conversion efficiency (PCE) due to a higher short circuit current (J_{sc}) than the OPV devices that used a nanowire-based transparent electrode. Silver nanowire mesh electrodes have been tested within P3HT/$PC_{61}BM$ cell architecture, and results comparable to these results and ITO standard cells have been observed previously.[1,22,23,32]

Model OPV devices on PET were prepared, cleaved, and briefly soaked in *o*-dichlorobenzene, a solvent that is selective for the bulk heterojunction (BHJ), with the goal of partially removing the BHJ to provide an unhindered view of the silver nanowire electrode. The model devices were assembled on PET and contained the following layers: PET/silver nanowires and PEDOT:PSS *or* PEDOT:PSS/P3HT:$PC_{61}BM$/Al. As can be seen in Figure 10a, the aluminum top electrode and the layers corresponding to the underlying PEDOT:PSS on the PET substrate are observed; the top Al electrode has not collapsed since there has been only partial removal of the P3HT:$PC_{61}BM$ BHJ. Figure 10b shows the model cell using an as-sprayed silver nanowire mesh on PET: In places, silver nanowires that are not parallel to the underlying PET substrate can be seen, suggesting the potential for shorting of the device. Figure 10c reveals the model device using the rolled silver nanowires (at 165 °C), in which the silver nanowire mesh appears topologically flat. Bridging silver nanowires could make contact between the PET and the aluminum top contact in the device, but the flattened mesh would not be expected to bridge the BHJ active layer.

4. CONCLUSIONS

Spraying of silver nanowire electrodes on PET is a straightforward and efficient approach for coating large areas of plastic and other substrates. Use of a rapid rolling pressure, of moderate intensity, combined with heat over the back of an as-sprayed silver nanowire mesh on plastic serves to weld the nanowires together, presses and flattens them down with respect to the surface, and brings about good adherence between the nanowires and the substrate surface. The sheet resistance of the nanowire mesh then drops substantially, below 20 Ω/□, and demonstrates high diffuse transmission of light ranging from 350 to 1200 nm. Repeated bending of rolled silver nanowire PET electrodes showed no degradation in sheet resistance, demonstrating good adhesion of the metal nanowires to the underlying substrate, presumably through a physical interaction that results from pressing the nanowires into the softened PET. This process could be integrated within a roll-to-roll process, in which the nanowire-on-plastic substrate is rolled between two rollers, one of which is heated. The approach described here should be generalizable to other metal

Table 5. Forward Mode OPV Devices Based upon Either ITO or Silver Nanowire Mesh-on-PET Electrodes, with the Following Architecture: Transparent Electrode/PEDOT:PSS/P3HT:$PC_{61}BM$/LiF/Al[a]

entry	electrode	short circuit current density (J_{sc}, mA/cm^2)	open circuit voltage (V_{oc}, V)	fill factor (FF)	efficiency (PCE, %)	series resistance (Ω·cm^2)	shunt resistance (kΩ·cm^2)	yield
1	ITO	8.7 ± 0.6	0.57 ± 0.01	0.59 ± 0.09	2.9 ± 0.3	6.7 ± 0.9	1.0 ± 0.5	100%
2	Ag mesh, not rolled	0	0	0	0	2.8 ± 11	0.003 ± 0.001	0%
3	Ag mesh, rolled	8.0 ± 0.6	0.57 ± 0.01	0.56 ± 0.02	2.5 ± 0.3	7.1 ± 1.0	1.1 ± 0.6	70%

[a]Ten devices were made and tested for each entry.

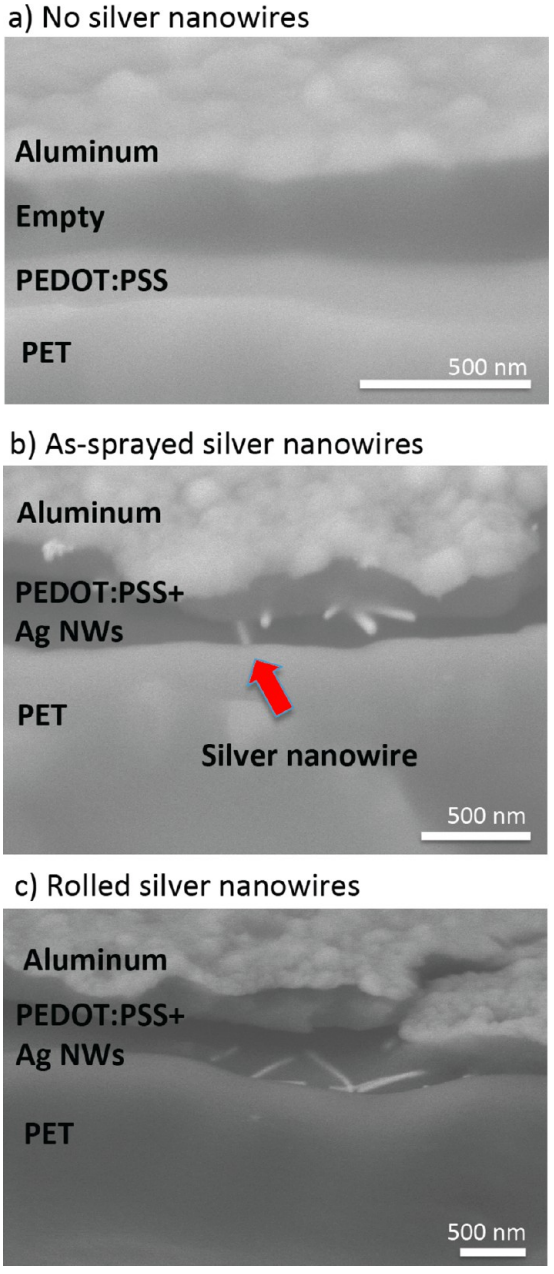

Figure 10. SEM images of cross-sectioned model OPV devices based upon the following architecture: PET/(PEDOT:PSS+Ag NWs *or* PEDOT:PSS)/P3HT:$PC_{61}BM$/Al. The model devices were briefly rinsed with *o*-dichlorobenzene to partially remove the P3HT:$PC_{61}BM$ bulk heterojunction to view the PEDOT:PSS/PET electrode.

nanowires (and possibly carbon-based nanomaterials) and a range of plastic substrates for applications beyond OPVs.

■ ASSOCIATED CONTENT

Ⓢ Supporting Information

Details and photographs regarding equipment and instrumentation, surface coverage and roughness calculations, and absolute UV−visible transmission profiles. This material is available free of charge via the Internet at http://pubs.acs.org.

■ AUTHOR INFORMATION

Corresponding Author

*E-mail: jburiak@ualberta.ca.

Notes

The authors declare no competing financial interest.

■ ACKNOWLEDGMENTS

Generous funding from Saudi Basic Industries (SABIC) is gratefully acknowledged. The Canadian Foundation for Innovation (CFI) and NSERC are thanked for their support.

■ REFERENCES

(1) Angmo, D.; Krebs, F. C. *J. Appl. Polym. Sci.* **2013**, *129*, 1−14.
(2) De, S.; King, P. J.; Lyons, P. E.; Khan, U.; Coleman, J. N. *ACS Nano* **2010**, *4*, 7064−7072.
(3) Liu, C. -H.; Yu, X. *Nanoscale Res. Lett.* **2011**, *6*, 75−83.
(4) Belenkova, T. L.; Rimmerman, D.; Mentovich, E.; Gilon, H.; Hendler, N.; Richter, S.; Markovich, G. *J. Mater. Chem.* **2012**, *22*, 24042−24047.
(5) Emmott, C. J. M.; Urbina, A.; Nelson, J. *Sol. Energy Mater. Sol. Cells* **2012**, *97*, 14−21.
(6) Chung, C.-H.; Song, T.-B.; Bob, B.; Zhu, R.; Yang, Y. *Nano Res.* **2012**, *5*, 805−814.
(7) Azzopardi, B.; Emmott, C. J. M.; Urbina, A.; Krebs, F. C.; Mutale, J.; Nelson, J. *Energy Environ. Sci.* **2011**, *4*, 3741−3753.
(8) Krebs, F. C.; Tromholt, T.; Jørgensen, M. *Nanoscale* **2010**, *2*, 873−886.
(9) Kyaw, A. K. K.; Tantang, H.; Wu, T.; Ke, L.; Peh, C.; Huang, Z. H.; Zeng, X. T.; Demir, H. V.; Zhang, Q.; Sun, X. W. *Appl. Phys. Lett.* **2011**, *99*, 021107−021110.
(10) Zhu, R.; Chung, C.-H.; Cha, K. C.; Yang, W.; Zhang, Y. B.; Zhou, H.; Song, T.-B.; Chen, C. -C.; Weiss, P. S.; Li, G.; Yang, Y. *ACS Nano* **2011**, *5*, 9877−9882.
(11) Mirri, F.; Ma, A. W. K.; Hsu, T. T.; Behabtu, N.; Eichmann, S. L.; Young, C. C.; Tsentalovich, D. E.; Pasquali, M. *ACS Nano* **2012**, *6*, 9737−9744.
(12) Becerril, H. A.; Mao, J.; Liu, Z.; Stoltenberg, R. M.; Bao, Z.; Chen, Y. *ACS Nano* **2008**, *2*, 463−470.
(13) Hecht, D. S.; Hu, L. B.; Irvin, G. *Adv. Mater.* **2011**, *23*, 1482−1513.
(14) O'Connor, B.; Haughn, C.; An, K. -H.; Pipe, K. P.; Shtein, M. *Appl. Phys. Lett.* **2008**, *93*, 223304−223307.
(15) Angmo, D.; Hosel, M.; Krebs, F. C. *Sol. Energy Mater. Sol. Cells* **2012**, *107*, 329−336.
(16) Hong, S.; Yeo, J.; Kim, G.; Kim, D.; Lee, H.; Kwon, J.; Lee, H.; Lee, P.; Ko, S. H. *ACS Nano* **2013**, *7*, 5024−5031.

(17) Hu, L.; Kim, H. S.; Lee, J. Y.; Peumans, P.; Cui, Y. *ACS Nano* **2010**, *5*, 2955−1963.
(18) Sun, Y.; Gates, B.; Mayers, B.; Xia, Y. *Nano Lett.* **2002**, *2*, 165−168.
(19) Lee, J. -Y.; Connor, S. T.; Cui, Y.; Peumans, P. *Nano Lett.* **2008**, *8*, 689−692.
(20) De, S.; Higgins, T. M.; Lyons, P. E.; Doherty, E. M.; Nirmalraj, P. N.; Blau, W. J.; Boland, J. J.; Coleman, J. N. *ACS Nano* **2009**, *7*, 1767−1674.
(21) Rathmell, A. R.; Nguyen, M.; Chi, M.; Wiley, B. J. *Nano Lett.* **2012**, *12*, 3193−3199.
(22) Sachse, C.; Muller-Meskamp, L.; Bormann, L.; Kim, Y. H.; Lehnert, F.; Philipp, A.; Beyer, B.; Leo, K. *Org. Electron.* **2013**, *14*, 143−148.
(23) Gaynor, W.; Burkhard, G. F.; McGehee, M. D.; Peumans, P. *Adv. Mater.* **2011**, *23*, 2905−2910.
(24) Gaynor, W.; Lee, J.-Y.; Peumans, P. *ACS Nano* **2010**, *4*, 30−34.
(25) Lee, J.-Y.; Connor, S. T.; Cui, Y.; Peumans, P. *Nano Lett.* **2010**, *10*, 1276−1279.
(26) Choi, D. Y.; Kang, H. W.; Sung, H. J.; Kim, S. S. *Nanoscale* **2013**, *5*, 977−983.
(27) Krantz, J.; Richter, M.; Spallek, S.; Spiecker, E.; Brabec, C. J. *Adv. Funct. Mater.* **2011**, *21*, 4784−4787.
(28) Zeng, X.-Y.; Zhang, Q.-K.; Yu, R.-M.; Lu, C.-Z. *Adv. Mater.* **2010**, *22*, 4484−4488.
(29) Akter, T.; Kim, W. S. *ACS Appl. Mater. Interfaces* **2012**, *4*, 1855−1859.
(30) Yu, Z.; Zhang, Q.; Li, L.; Chen, Q.; Niu, X.; Liu, J.; Pei, Q. *Adv. Mater.* **2011**, *23*, 664.
(31) Yang, L.; Zhang, T.; Zhou, H.; Price, S. C.; Wiley, B. J.; You, W. *ACS Appl. Mater. Interfaces* **2011**, *3*, 4075−4084.
(32) Yu, Z.; Li, L.; Zhang, Q.; Hu, W.; Pei, Q. *Adv. Mater.* **2011**, *23*, 4453−4457.
(33) Kim, A.; Won, Y.; Woo, K.; Kim, C. -H.; Moon, J. *ACS Nano* **2013**, *7*, 1081−1091.
(34) Mehra, S.; Christoforo, M. G.; Peumans, P.; Salleo, A. *Nanoscale* **2013**, *5*, 4400−4403.
(35) Stubhan, T.; Krantz, J.; Li, N.; Guo, F.; Litzov, I.; Steidl, M.; Richter, M.; Matt, G. B.; Brabec, C. J. *Sol. Energy Mater. Sol. Cells* **2012**, *107*, 248−251.
(36) Gan, Q.; Bartoli, F. J.; Kafafi, Z. H. *Adv. Mater.* **2013**, *25*, 2385−2396.
(37) Garnett, E. C.; Cai, W.; Cha, J. J.; Mahmood, F.; Connor, S. T.; Christoforo, M. G.; Cui, Y.; McGehee, M. D.; Brongersma, M. L. *Nat. Mater.* **2012**, *11*, 241−249.
(38) Madiara, A. R.; Kumar, A.; Ishikawa, F. N.; Zhou, C. *Nano Res.* **2010**, *3*, 564−573.
(39) De, S.; Coleman, J. N. *ACS Nano* **2010**, *4*, 2713−2710.